

Comparison of immersion and side cooling systems of cylindrical Li-Ion cells

Jiri Hvozda^{1*}, Jan Bohacek¹, and Miroslav Raudensky¹

¹Heat Transfer and Fluid Flow Laboratory, Faculty of Mechanical Engineering, Brno University of Technology, Technicka 2896/2, 616 69 Brno, Czechia

Abstract. The safety and durability of Li-Ion batteries strongly depend on effective thermal management, especially under high C-rate operation. This work presents a comparative numerical investigation of immersion and side cooling applied to cylindrical 18650 cells. A transient three-dimensional model was developed for a series-connected pack of nine cells subjected to a 3.8 C discharge rate. Heat generation was implemented through a source term defined as a function of temperature and discharge time, enabling a realistic yet computationally straightforward representation of electro-thermal behaviour. The two cooling strategies were systematically assessed with respect to coolant flow rate, focusing on maximal temperature and temperature spread across the pack. The results show that both immersion and side cooling achieve nearly identical thermal performance in terms of maximal temperature and temperature spread. However, side cooling suffers from a higher pressure drop, whereas immersion cooling places stricter demands on the sealing and dielectric properties of the coolant. Overall, the study demonstrates that each method has specific trade-offs, and the optimal choice depends on the balance between thermal performance, hydraulic losses, and design complexity.

1 Introduction

Temperature control is a key requirement in the operation of Li-Ion batteries, particularly under high load conditions where internal heat generation intensifies. Heat is produced through a combination of Ohmic losses, concentration polarisation, and activation processes, and insufficient heat removal can lead to a range of adverse effects, including accelerated capacity fade, increased self-discharge, electrical imbalance, and, in extreme cases, thermal runaway. To ensure safe and reliable operation, Li-Ion cells are typically kept within an operating window of 15–35 °C, while the temperature spread within a module is generally recommended to remain below 5 °C to avoid uneven ageing and mismatched discharge behaviour between cells [1, 2]. A variety of battery thermal management systems (BTMS) exist, ranging from simple air-cooled designs to liquid cooling, heat pipes, phase-change materials, or hybrid systems combining several mechanisms. Among these, liquid-based cooling seems to offer the most favourable balance of heat-removal capacity and packaging flexibility for high-performance applications such as electric vehicles. Conventional designs rely on aluminium cold plates or serpentine channels, but these add weight and rely on materials with a high carbon footprint. In comparison, extruded polymers generate roughly four times less CO₂ per kilogram than aluminium [3], making polymer-based heat exchangers an attractive alternative when weight and sustainability are considered.

Recent advances in polymeric heat exchangers have demonstrated that their thermal performance can approach that of traditional metal-based systems when designed with thin walls and large heat-transfer areas [4]. A notable example is the hollow fiber heat exchanger architecture developed by Boháček et al.,

where polypropylene hollow fibers were embedded within a rigid polydicyclopentadiene housing [5]. This concept was successfully demonstrated for cooling of 18650 Li-Ion cells and later refined into a more modular configuration suitable for integration into battery modules [6] and will be further compared in this study. In parallel, immersion cooling has emerged as another promising thermal management approach. By fully submerging cells in a dielectric liquid, this method eliminates thermal interface resistances and cools the entire external surface of each cell. However, immersion systems also require complete sealing of the battery compartment and careful consideration of fluid compatibility, long-term stability, and system integration [7].

In this study, we numerically compare these two cooling approaches (i) polymeric hollow fiber side cooling and (ii) full immersion cooling applied to a pack of nine cylindrical 18650 Li-ion cells discharged at 3.8 C. A transient three-dimensional CFD model is used to evaluate the resulting temperature fields, maximal temperatures, and thermal uniformity across a range of coolant flow rates. The results highlight the relative benefits and limitations of each geometry and provide insight for designing efficient, lightweight, and electrically safe BTMS solutions.

2 Methods

The studied battery module consists of nine cylindrical Li-Ion 18650 cells with a nominal capacity of 2.6 Ah connected in series and arranged in two parallel rows, with four cells in one row and five in the other. The coolant flows along a meandering channel formed between and around the batteries. A symmetry plane is introduced through the mid-planes of all nine cells, so

* Corresponding author: Jiri.Hvozda@vut.cz

the computational domain contains all batteries but only one half of their geometry. This reduces computational cost while preserving the whole thermal interaction between the cells and the coolant. Two cooling concepts are evaluated under comparable operating conditions.

In the first configuration, the dielectric liquid flows inside a polymeric hollow fiber heat exchanger. The exchanger consists of polypropylene micro-tubes embedded in a durable polydicyclopentadiene skeleton, and a thermally conductive paste is placed between the batteries and the exchanger to ensure good thermal contact. In the second configuration, the batteries are fully immersed in the same dielectric liquid, which directly wets all external cell surfaces. The inlet temperature and volumetric flow rates are identical for both configurations; however, because the available flow cross-sections differ, the resulting coolant velocities are not the same. This setup enables a fair comparison of the two cooling strategies based solely on their heat-transfer geometry and resulting thermal and hydraulic performance.

2.1 Governing equations

The thermal behaviour of the battery pack and fluid domain was modelled using a three-dimensional transient model solving the conservation equations of mass, momentum, and energy. The cooling medium was treated as an incompressible Newtonian fluid. The Reynolds number was below 2000 in all cases, and thus the flow was considered laminar. The thermal conductivity of cylindrical batteries is considered to be cyclic orthotropic with constant values of radial, tangential and axial terms, which are further denoted as k_{rad} , k_{tan} , and k_{ax} , respectively. The source term inside the conservation of energy equation is the sum of irreversible (S_{irr}) and reversible (S_{rev}) heat generation rates which are associated with Joule's heating and change of entropy inside the battery, respectively, as a function of discharging current, temperature and time. The governing equations follow based on [8] as

$$\nabla \cdot \mathbf{v} = 0, \quad (1)$$

$$\frac{\partial \mathbf{v}}{\partial t} + (\mathbf{v} \cdot \nabla) \mathbf{v} = -\frac{1}{\rho} \nabla p + \nu \nabla^2 \mathbf{v}, \quad (2)$$

$$\rho c_p \frac{\partial T}{\partial t} + \rho c_p (\mathbf{v} \cdot \nabla T) = \nabla \cdot (K_{\text{car}} \nabla T) + S \quad (3)$$

Where \mathbf{v} is a velocity vector, t is time ρ is density, p is pressure, ν is kinematic viscosity, c_p is specific heat capacity, T is temperature, K_{car} is a tensor of thermal conductivity in Cartesian coordinates, and S is the source term. For the materials other than the battery, the thermal conductivity tensor is simplified to a constant value. For the Li-Ion battery 18650, the thermal conductivity tensor in Cartesian coordinates is obtained from a transformation from local values in cylindrical coordinates as

$$K_{\text{car,bat}} = \Sigma K_{\text{cyl,bat}} \Sigma^T, \quad (4)$$

where

$$\Sigma = \begin{bmatrix} \cos \varphi & -\sin \varphi & 0 \\ \sin \varphi & \cos \varphi & 0 \\ 0 & 0 & 1 \end{bmatrix}, \quad (5)$$

$$K_{\text{cyl,bat}} = \begin{bmatrix} k_{\text{rad}} & 0 & 0 \\ 0 & k_{\text{tan}} & 0 \\ 0 & 0 & k_{\text{ax}} \end{bmatrix}, \quad (6)$$

The angle φ is determined by the deviation by the line going through points $(0, 0, z_0)$ and $(1, 0, z_0)$ and the line connecting a point (x_0, y_0, z_0) and the point $(0, 0, z_0)$, for every point (x_0, y_0, z_0) inside the cylindrical battery domain with origin in the centre of its circular cross-section.

Further, for a constant discharging current I within a battery of volume V , the source partial terms following the methodology in [9] can be written as

$$V \cdot S_{\text{irr}} = I^2 R, \quad (7)$$

$$V \cdot S_{\text{rev}} = -I \left(T \left(\frac{dE}{dT} \right) \right), \quad (8)$$

where internal resistance (R) and change of entropy with respect to temperature (dE/dT) are polynomials in the form of

$$R = \sum_{i=0}^m \sum_{j=0}^n r_{ij} \cdot (\text{SOC})^i \cdot T^j, \quad (9)$$

$$\frac{dE}{dT} = \sum_{i=0}^m e_i \cdot (\text{SOC})^i, \quad (10)$$

for some natural numbers m, n . The coefficients are obtained experimentally by discharging the batteries with different currents at various surrounding temperatures. The time dependency in the previous terms is implicitly given by SOC (state of charge), which is defined as

$$\text{SOC} = 1 - C \cdot \frac{t}{3600}, \quad (11)$$

where C is the C-rate, which corresponds to the inverse of the total discharging (respective charging) time in hours, for instance, discharging a battery at C-rate of 0.5 means that the battery will be fully discharged in 2 hours. Particular values of the coefficient in equations (9) and (10) are given in Table 1.

Table 1. Parameters of the polynomials inside the source term in the conservation of energy equation [9].

i	r_{i0}	r_{i1}	r_{i2}	r_{i3}	e_i
0	0.024	0.0013	$-6.1 \cdot 10^{-6}$	$7.5 \cdot 10^{-9}$	$-3.4 \cdot 10^{-4}$
1	-0.189	$-1.4 \cdot 10^{-4}$	$7.4 \cdot 10^{-7}$	0	$9.79 \cdot 10^{-4}$
2	0.301	$-2.0 \cdot 10^{-4}$	0	0	$-1.5 \cdot 10^{-3}$
3	-0.11	0	0	0	$7.41 \cdot 10^{-4}$

2.2 Computational domains

A three-dimensional representation of the heat exchanger with five inserted cells is shown in Fig. 1. The hollow fibers have an inner diameter of 0.8 mm and an outer diameter of 1 mm. Due to the symmetric arrangement of the fiber layers and battery rows, it is sufficient to model only one half of the two battery rows. The corresponding height of the modelled domain is 2 mm, which reflects the symmetry plane and

simultaneously matches the periodic structure defined by the 0.8 mm spacing between adjacent fibers. A thermally conductive paste is placed between the batteries and the heat exchanger to ensure efficient thermal contact and eliminate potential gaps. The thermophysical properties of all materials are given in Table 2.

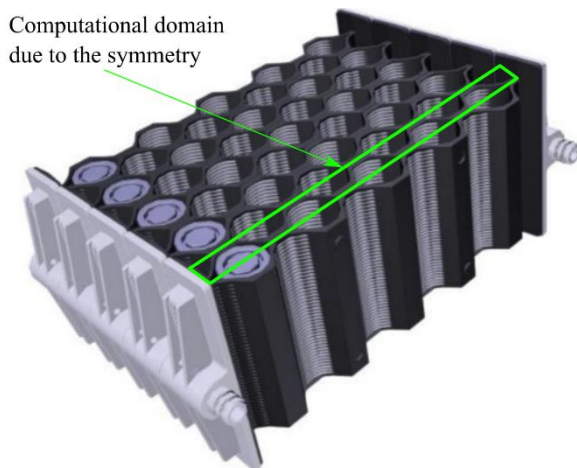


Fig. 1. A polymeric heat exchanger with hollow fibers as coolant channels with a few of Li-Ion cells 18650 inserted with computational domain [6].

The same reduced geometry is also used for the immersion-cooling configuration. In this case, all domains except the batteries are replaced by a single fluid region filled with dielectric liquid, while keeping the battery positions and spacing identical. This approach enables a direct comparison of the two cooling strategies using an identical computational domain, differing only in the nature of the surrounding cooling medium. Both geometries are visualised in Fig. 2

The boundary conditions are identical for both configurations. A uniform inlet velocity is prescribed at the coolant inlet. The volumetric flow rate varies between 0 and 10 l·h⁻¹, which corresponds to inlet velocities between 0 and 0.11 m·s⁻¹ in the side-cooling configuration and between 0 and 0.024 m·s⁻¹ in the immersion-cooling configuration, reflecting the different flow cross-sections of the two geometries. The inlet temperature is fixed at 20 °C. The outlet boundary condition is set to 0 Pa pressure, while all remaining external faces of the domain are treated as symmetry boundaries. The initial temperature of all domains, including the batteries, heat exchanger materials, thermally conductive paste and dielectric fluid, is set to 20 °C.

A constant discharging current of 10 A (corresponding to a 3.8 C rate) is applied to all nine cells. The simulations are run until a terminal physical time of 936 s, which corresponds to the time needed for the cells to fully discharge under the applied current.

Table 2. Thermophysical properties of the materials.

Property	Value	Unit
Dielectric fluid [10]		
ρ	810	(kg m ⁻³)
c_p	1850	(J kg ⁻¹ K ⁻¹)
k	0.13	(W m ⁻¹ K ⁻¹)
ν	$0.58 \cdot 10^{-5}$	(m ² s ⁻¹)
Polypropylene [11]		
ρ	895	(kg m ⁻³)
c_p	1920	(J kg ⁻¹ K ⁻¹)
k	0.19	(W m ⁻¹ K ⁻¹)
Thermally conductive paste [12]		
ρ	3100	(kg m ⁻³)
c_p	1100	(J kg ⁻¹ K ⁻¹)
k	3.5	(W m ⁻¹ K ⁻¹)
Polydicyclopentadiene [13, 14]		
ρ	1040	(kg m ⁻³)
c_p	1600	(J kg ⁻¹ K ⁻¹)
k	0.17	(W m ⁻¹ K ⁻¹)
Cylindrical battery 18650 [15–17]		
ρ	2362	(kg m ⁻³)
c_p	1720	(J kg ⁻¹ K ⁻¹)
k	$\begin{bmatrix} 0.5 & 0 & 0 \\ 0 & 30 & 0 \\ 0 & 0 & 30 \end{bmatrix}$	(W m ⁻¹ K ⁻¹)

3 Results

To quantitatively evaluate the thermal performance of both cooling concepts, two key temperature indicators are used: (1) Maximal cell temperature (T_{\max}), which is defined as the highest temperature within the battery pack at the terminal simulation time. This value is a critical parameter for assessing thermal safety and overall cooling effectiveness. (2) Maximal temperature spread (ΔT_{\max}) is the difference between the highest and lowest cell temperatures within the battery pack at the same time instant. This metric describes temperature non-uniformity, which is directly linked to unequal ageing, electrical imbalance, and long-term reliability of the battery module. Both quantities are extracted from the solid domain of the cells and evaluated at the terminal time of 936 s, corresponding to full discharge at a 3.8 C rate. Both parameters, together with the pressure drop, are summarised in Table 3 for both configurations.

In the immersion-cooling configuration, the maximal temperature without flow is 61.82 °C with a small temperature spread ($\Delta T = 3.86$ °C). At flowrate of 0.34 l·h⁻¹, the maximal temperature remains high at 61.76 °C. However, the temperature spread increases substantially to 27.11 °C because the slowly moving dielectric liquid heats up rapidly along the flow path and cools down only the first battery. As the flow rate increases, the maximal temperature decreases to 52.66 °C at 1.35 l·h⁻¹, 46.29 °C at 2.69 l·h⁻¹, and 42.92 °C at 4.49 l·h⁻¹. At the highest tested flow rate of

10 l·h⁻¹, immersion cooling achieves a maximal temperature of 39.86 °C with a maximal temperature spread of 15.41 °C.

In the side-cooling configuration, heat is extracted indirectly through the polymeric hollow fiber heat exchanger. Without flow, the maximal temperature reaches 60.16 °C with a temperature spread of 6.87 °C. As coolant flow increases, the maximal temperature decreases progressively: to 54.91 °C at 1 l·h⁻¹, 48.21 °C at 2 l·h⁻¹, and 41.73 °C at 5 l·h⁻¹. At 10 l·h⁻¹, side cooling reaches a maximal temperature of 39.09 °C with a maximal temperature spread of 15.28 °C. Essentially, it matches the thermal performance of immersion cooling at the same flow rate.

The dominant difference between the two approaches lies not in their thermal effectiveness, but in their hydraulic behaviour. Immersion cooling operates with very low pressure losses (33.5 Pa at 10 l·h⁻¹), whereas side cooling exhibits 100x higher hydraulic resistance due to microchannel confinement (3096 Pa at 10 l·h⁻¹).

Table 3. Numerical results.

Immersion cooling			
Φ l · h ⁻¹	T_{\max} °C	ΔT_{\max} °C	ΔP Pa
0	61.82	3.86	0.00
0.34	61.76	27.11	1.24
0.67	59.05	28.11	2.49
1.35	52.66	28.60	4.98
2.69	46.29	19.45	9.97
4.49	42.92	17.18	16.64
10	39.86	15.41	33.54
Side cooling			
Φ l · h ⁻¹	T_{\max} °C	ΔT_{\max} °C	ΔP Pa
0	60.16	6.87	0.00
0.075	59.94	14.13	23.15
0.15	60.04	20.25	46.31
1	54.91	27.91	308.79
2	48.21	22.70	617.71
5	41.73	17.34	1545.40
10	39.09	15.28	3095.65

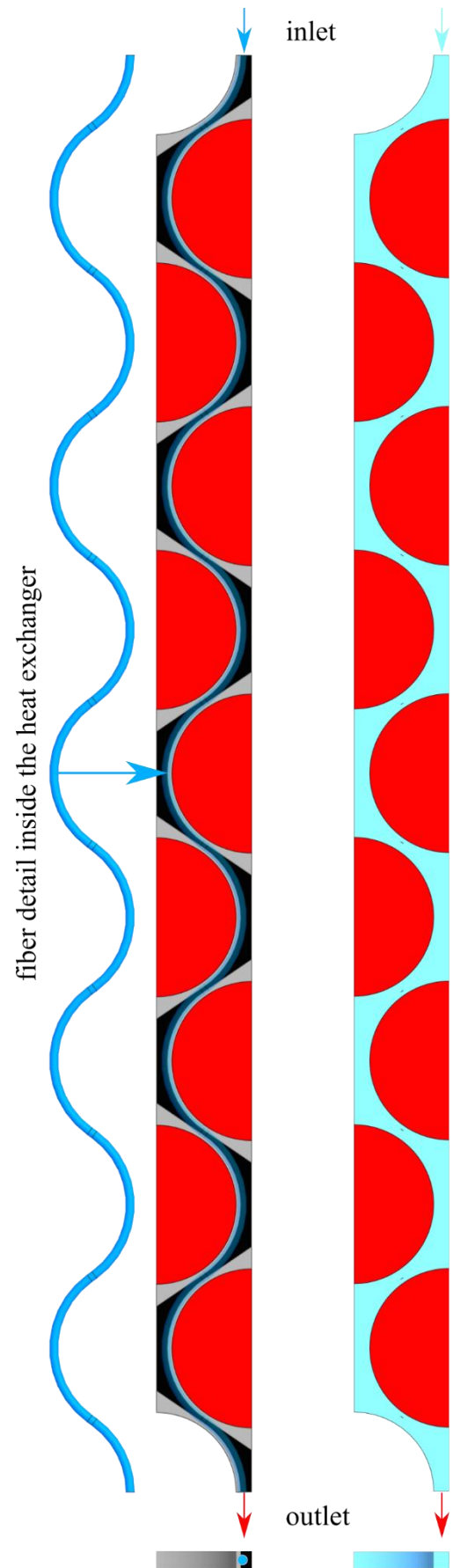


Fig. 2. Illustration of the computational domains of side (left) and immersion (right) cooling. The side cooling case includes the details on the fluid domain shape. Due to the complexity of the geometry, the full 3D models are provided in [18].

4 Conclusions

This work presented a comparative numerical study of immersion cooling and polymeric hollow fiber side cooling applied to a 9-cell cylindrical 18650 Li-Ion battery module discharging at 3.8 C. A transient three-dimensional model incorporating temperature- and SOC-dependent heat generation was used to evaluate thermal behaviour and hydraulic performance across a wide range of coolant flow rates.

The results demonstrate that neither cooling strategy is able to maintain low or uniform cell temperatures at this high C-rate. Even at the highest coolant flow of $10 \text{ l}\cdot\text{h}^{-1}$, both configurations exhibit maximum temperatures close to $40 \text{ }^\circ\text{C}$ and a temperature spread of approximately $15 \text{ }^\circ\text{C}$, which exceeds typical recommendations for long-term battery health. This clearly indicates that the dominant thermal limitation does not lie in the design of the heat exchanger, but rather in the intrinsically low radial thermal conductivity of cylindrical Li-Ion cells, which restricts heat removal from the internal core. As a consequence, modifications to the external cooling geometry can only partially improve performance at high load conditions. Despite their different geometries and heat-transfer mechanisms, immersion and side cooling behave nearly identically with respect to the maximal temperature and temperature spread.

Immersion cooling requires complete sealing of the battery thermal management system, which increases design complexity and imposes stricter demands on manufacturing and long-term reliability. Side cooling, by contrast, provides a structurally protected and mechanically separated coolant circuit. A major distinction between the two concepts emerges in their hydraulic behaviour. Immersion cooling requires only minimal pumping power, with pressure drops below 40 Pa at $10 \text{ l}\cdot\text{h}^{-1}$. Side cooling, however, exhibits pressure losses exceeding 3000 Pa at the same flow rate due to microchannel geometry. Thus, although their thermal performance becomes nearly identical, their hydraulic requirements and system-integration implications differ substantially.

The results demonstrate that, for the same coolant flow rate, immersion cooling and side cooling deliver almost identical maximum temperatures and temperature spreads, despite their different geometries and heat-transfer mechanisms. This indicates that, under high C-rate operation, the dominant thermal limitation arises from the intrinsically low radial thermal conductivity of cylindrical 18650 cells, not from the external cooling architecture. As a consequence, further improvements in thermal performance at such load conditions cannot be achieved solely by redesigning the surrounding heat exchanger. Meaningful progress will require solutions that address the internal thermal bottleneck of the cell itself, including enhanced intra-cell heat conduction, alternative cell formats, or hybrid thermal-management strategies.

This work was supported by projects "The Energy Conversion and Storage", funded as project No. CZ.02.01.01/00/22_008/0004617 by Programme Johannes

Amos Comenius, call Excellent Research and "Hollow Fiber Heat Exchangers with Reduced Permeability for Smart Cities", funded as project No. 8I24002 by Programme EIG CONCERT by Ministry of Education, Youth and Sports.

Jiri Hvozda contributed to conceptualisation, methodology, writing—original draft and writing—review and editing. Jan Bohacek contributed to conceptualisation, methodology, writing—review and editing. Miroslav Raudensky contributed to supervision, writing—review and editing.

The data that support the findings of this study are openly available in the Dataset for Comparison of Immersion and Side Cooling Systems of Cylindrical Li-Ion Cells at <https://doi.org/10.5281/zenodo.17868718>, reference number [18]

References

1. Q.L. Yue, C.X. He, M.C. Wu, T.S. Zhao, Advances in thermal management systems for next-generation power batteries. *Int. J. Heat Mass Transf.* **181**, 121853 (2021). <https://doi.org/10.1016/j.ijheatmasstransfer.2021.121853>.
2. Z. Rao, S. Wang, A review of power battery thermal energy management. *Renew. Sustain. Energy Rev.* **15**, 4554–4571 (2011). <https://doi.org/10.1016/j.rser.2011.07.096>.
3. The Greenhouse Gases, Regulated Emissions, and Energy Use in Technologies (GREET®) Model. Argonne National Laboratory (2021). Available at: <https://greet.es.anl.gov/>
4. J. Hvozd'a, K. Mráz, M. Raudenský, A. Vakhrushev, E. Karimisibaki, J. Boháček, Case Study on Thermal Management of Planar Elements with Various Polymeric Heat Exchangers: Experiment and Simulation. *J. Therm. Anal. Calorim.* **149**, 5229–5238 (2024). <https://doi.org/10.1007/s10973-024-13172-x>.
5. J. Boháček, M. Raudenský, E. Karimi-Sibaki, Polymeric hollow fibers: Uniform temperature of Li-ion cells in battery modules. *Appl. Therm. Eng.* **159**, 113940 (2019). <https://doi.org/10.1016/j.applthermaleng.2019.113940>.
6. J. Boháček, J. Hvozd'a, K. Mráz, A. Vakhrushev, E. Karimisibaki, Polymeric hollow fibers: a modular heat exchanger for thermal management systems of battery modules in electric vehicles. In: *Proc. EFM21 – 15th Int. Conf. Experimental Fluid Mechanics 2021*, Liberec, Czechia, Nov 23–26, 2021. *EPJ Web Conf.* **264**, 01005 (2022). <https://doi.org/10.1051/epjconf/202226401005>.
7. X. Zhang, Z. Li, L. Luo, Y. Fan, Z. Du, A review on thermal management of lithium-ion batteries for electric vehicles. *Energy* **238**, 121652 (2022). <https://doi.org/10.1016/j.energy.2021.121652>.
8. F.H. Moukalled, L. Mangani, M. Darwish, *The Finite Volume Method in Computational Fluid Dynamics: An Advanced Introduction with OpenFOAM and Matlab* (Springer, Cham, 2016).

9. J. E, et al., Effects of the different air cooling strategies on cooling performance of a lithium-ion battery module with baffle. *Appl. Therm. Eng.* **144**, 231–241 (2018). <https://doi.org/10.1016/j.applthermaleng.2018.08.064>.
10. FUCHS Lubricants. Single Phase Immersion Cooling Fluids. Available at: <https://www.fuchs.com/us/en/single-phase-immersion-cooling-fluids/>.
11. M. Gahleitner, C. Paulik, Polypropylene and other polyolefins. In: *Brydson's Plastics Materials* (Butterworth-Heinemann, 2017), 279–309. <https://doi.org/10.1016/B978-0-323-35824-8.00011-6>.
12. Momentive Performance Materials. SilCool™ TIA350R Adhesive. Available at: <https://www.momentive.com/en-us/categories/adhesives-and-sealants/silcooltia350r-adhesive>.
13. P.Y. Le Gac, D. Choqueuse, M. Paris, G. Recher, C. Zimmer, D. Melot, Durability of polydicyclopentadiene under high temperature, high pressure and seawater. *Polym. Degrad. Stab.* **98**, 809–817 (2013). <https://doi.org/10.1016/j.polymdegradstab.2012.12.023>.
14. I.D. Robertson, et al., Rapid energy-efficient manufacturing of polymers and composites via frontal polymerisation. *Nature* **557**, 223–227 (2018). <https://doi.org/10.1038/s41586-018-0054-x>.
15. S. Drake, D. Wetz, J. Ostatek, S. Miller, J. Heinzl, A. Jain, Measurement of anisotropic thermophysical properties of cylindrical Li-ion cells. *J. Power Sources* **252**, 298–304 (2014). <https://doi.org/10.1016/j.jpowsour.2013.11.107>.
16. M. Tousi, A. Sarchami, M. Kiani, M. Najafi, E. Houshfar, Numerical study of a novel liquid-cooled thermal management system for cylindrical Li-ion battery packs under high discharge rate. *J. Energy Storage* **41**, 102910 (2021). <https://doi.org/10.1016/j.est.2021.102910>.
17. M. Al-Zareer, A. Michalak, C. da Silva, C.H. Amon, Predicting specific heat capacity and directional thermal conductivities of cylindrical lithium-ion batteries: A combined experimental and simulation framework. *Appl. Therm. Eng.* **182**, 116075 (2021). <https://doi.org/10.1016/j.applthermaleng.2020.116075>.
18. Hvozda, J., Bouzek, K., & Paušová, Š. (2025). Dataset for Comparison of Immersion and Side Cooling Systems of Cylindrical Li-Ion Cells (version 1) [Data set]. Zenodo. <https://doi.org/10.5281/zenodo.17868718>.